Spatial Imaging of Singlet Energy Migration in Perylene Bis(phenethylimide) Thin Films

David M. Adams,[†,§] Josef Kerimo,[‡] Donald B. O'Connor,[†] and Paul F. Barbara*,[†]

Department of Chemistry and Biochemistry, University of Texas at Austin, Austin, Texas, 78712, and
Department of Chemistry, University of Minnesota, Minneapolis, Minnesota, 55455

Received: June 25, 1999; In Final Form: September 23, 1999

The migration length of singlet electronic energy excitations (excitons) in thin films of perylene bis-(phenethylimide) (PPEI) has been measured by an imaging technique that incorporates near-field optical excitation and far-field fluorescence imaging. The observed energy migration lengths fall in the range of ≤50 to ∼500 nm depending on sample morphologies. Sample morphology was controlled by "solvent annealing" and characterized by fluorescence NSOM and scanning force microscopy. The potential role of sample morphology in singlet energy migration is discussed. Additionally, the results reported herein are compared with a previous determination of singlet energy migration in PPEI.

Introduction

Diffusion of electronic energy (excitons) within layers of organic multilayer heterostructures is a critical process in organic solar cells and organic light emitting diodes.[1−4] For example, consider a typical organic solar cell (Figure 1) comprised of a multilayer structure involving an organic heterojunction of the visible absorbing layer bis(phenethylimide) (PPEI)[5−10] and the *p*-type organic semiconductor layer polymethylthiophene (PMT). The charges are conducted to the external circuit by the Al and ITO electrodes. Electronic energy absorbed by the PPEI layer must migrate to the PPEI/PMT interface where the necessary charge separation occurs. The energy diffusion length of excitons L_D must be at least as large as the layer thickness for charge separation to be efficient. The one-dimensional singlet exciton migration length is a competition between the rate of energy migration and the electronic decay rate, τ_s^{-1}, of the singlet exciton, as follows:

$$L_D = \sqrt{D_s \tau_s} \tag{1}$$

where τ_s is the lifetime of singlet excitons and D_s is the diffusion constant.[11,12]

For a given material, L_D has been observed to vary tremendously due to several factors.[13] First, the presence of trace impurities can "trap" singlet excitons and thus diminish D_s.[5,14] Some impurities can also act as fluorescence quenchers, thereby leading to significantly shorter τ_s. Organic thin film morphology is another potential controlling factor for L_D. Vapor-deposited organic thin films of aromatic molecules such as PPEI can exist in a broad range of morphologies ranging from a uniform amorphous material to locally microcrystalline composite depending on deposition and processing conditions.[4,5,7−10,15−18] Furthermore, the different microcrystals in a sample typically exist in a distribution of crystal morphologies.[7,8]

The most popular method for measuring L_D involves a bilayer structure comprised of the material of interest (optical absorber)
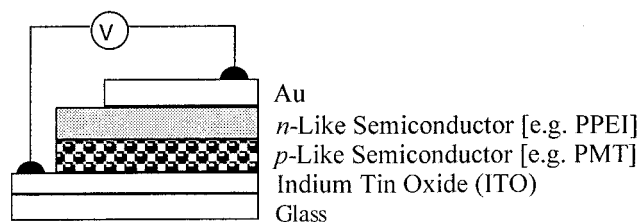

Figure 1. Schematic of typical organic semiconductor-based solar cell.

in contact with a quenching layer (quenching via energy, electron, or hole transfer). The absorbing layer is optically excited on the side of the sample opposite the quenching layer, producing a spatial distribution of optical excitation in the sample as a function of displacement in the absorbing layer along the direction perpendicular to the absorber/acceptor plane. The spatial distribution of optical excitation in the absorbing layer is varied in this technique by varying the excitation wavelength, which alters the penetration depth, and/or by varying the sample thickness. The fluorescence yield as a function of excitation wavelength and/or absorber layer thickness can be modeled to determine L_D.[6,19]

The model used to determine the L_D values from the florescence quenching data is based on a mechanism composed of two distinct processes. The first process involves the diffusion of a singlet exciton through the absorbing layer. The second process involves the quenching of the exciton at the absorber/quencher layer. The observable of the experiment, the fluorescence quenching efficiency, is a product of the efficiencies of both of these stages. The data analysis method used does not permit the independent determination of the rate or efficiency of either of the two processes. To derive the rate of diffusion of the exciton through the absorbing layer, it has often been assumed that the rate of quenching at the absorber/quencher interface is infinity. Using this approximation, the majority of L_D values for organic materials have been reported to be in the range 30−300 nm.[13,20−22] Since the actual quenching rate at the interface is smaller, the L_D values determined from this method may be smaller than the actual values. For example, for exciton migration in anthracene crystals at room temperature,[23−25] the reported L_D values vary by 2−3 orders of magnitude with one reported value as large as 900 nm.[24] Kenkre

* To whom correspondence should be addressed.
† University of Texas.
‡ University of Minnesota.
§ Current address: Department of Chemistry, Columbia University, New York 10027.

Perylene Bis(phenethylimide) Thin Films

J. Phys. Chem. A, Vol. 103, No. 49, 1999 **10139**
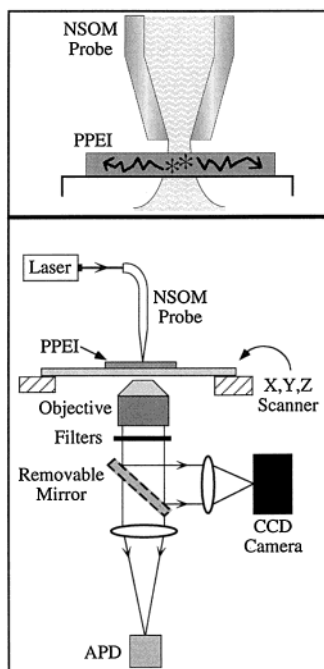
Figure 2. Experimental setup for far field/near field fluorescence imaging of PPEI microcrystals.

et al.[13] have shown that this tremendous variation is due to the inadequacy of assuming a quenching rate of infinity at the absorber/quencher interface.

In the present paper we employ an alternative technique to measure L_D for solvent vapor annealed PPEI. This material has been reported to have extraordinarily long-range exciton diffusion, i.e., $L_D = (2.5 \pm 0.5) \mu$m.[6] This long diffusion length is not simply a function of a long excited-state lifetime. In fact, τ_s for PPEI is shorter than many organic materials, and the calculated value for D_s based on $L_D = 2.5 \mu$m, i.e., $D_s \approx 180$ cm^2/s is much larger than that reported for other organics. In the new approach in this paper, PPEI is excited with a near-field optical probe with an optical field diameter of ∼50 nm. This allows for spatially resolved excitation of the sample including the excitation of individual microcrystals. The energy diffusion in the sample plane is measured by imaging the fluorescence in the far field with a CCD camera and a microscope objective at high magnification. Due to diffraction, the "spot size" of the imaged fluorescence is greater than or equal to the diffraction limit, ∼350 nm for PPEI emission, in our apparatus. Using convolution methods the data can be analyzed to measure diffusion lengths as small as 50 nm. A related imaging technique employing time-resolved luminescence measurements has been utilized to determine L_D for excitons in GaAs quantum wells.[26]

Apparatus and Experimental Procedures

Thin films of PPEI on glass, indium tin oxide (ITO) coated glass, and polymethylthiophene(∼100 nm)/ITO/glass multilayers were prepared by previously described methods.[6,8]

PPEI films were optically excited through a standard Al coated, tapered NSOM probe with an optical near field diameter of ∼50 nm (Figure 2). Samples were excited with either 488 nm (cw Ar$^+$ laser, OmNichrome 543R-A-AO3) or 543.5 nm (cw green Helium Neon laser, Melles Griot 05-LGR-193). Typically, less than 0.5 mW of unpolarized excitation light was coupled into the optical probe fiber. Short-pass (900 nm), long-pass (typically 550 nm), as well as narrow band-pass (680 nm

for data in Figures 3 and 4) filters were placed in the optical path between the objective and detector to block excitation light and scattered feedback laser light (980 nm) while transmitting PPEI fluorescence.

The experimental apparatus (Figure 2) is similar to that described earlier.[27−29] With the removable mirror out of the optical path, the instrument is a fluorescence NSOM apparatus based on Aurora (TopoMetrix) commercial NSOM instrument. The fluorescence from the sample is monitored by an avalanche photodiode in the NSOM configuration, and the sample is raster scanned. Simultaneous with the fluorescence NSOM image, a shear-force image is also acquired. The shear-force image is a measure of the topography of the sample. All experiments were carried out at room temperature.

For spatial imaging of singlet energy migration the sample is moved by the *xy*-stage in order to position the optical probe over a chosen sample region. The shear-force feedback system maintains a tip/sample distance of ∼7.5 nm. With the removable mirror in the optical beam path the PPEI fluorescence from the chosen region of the sample is optically imaged at a magnification 300X or alternatively 250X (objectives 1 and 2 respectively; see below) by a LN$_2$-cooled CCD camera with a pixel size of 25 μm. The spatial profile of singlet energy diffusion is monitored in the far field by the imaging CCD camera. The magnification at the CCD was determined by imaging a 40 μm grid.

As a resolution standard for the energy diffusion measurements, a far-field image was recorded with the CCD camera of the 633 nm light emitted from the NSOM probe with a 633 nm HeNe laser coupled into the NSOM fiber. The images of the PPEI fluorescence and the HeNe 633 nm reference images were taken under identical optical arrangements. This was accomplished by coupling both HeNe and excitation light into the NSOM probe. With the tip in feedback very near the surface, the excitation beam was blocked from entering the NSOM fiber and the HeNe image recorded. The HeNe was then blocked, excitation light passed to tip and fluorescence image recorded.

Two microscope objectives were employed in these measurements. Objective 1 was an oil immersion (NA = 1.2, 100X, Zeiss achromat) which leads to a nearly diffraction limited spot of 350 nm and allowed for determination of L_D down to ∼50 nm using a convolution procedure. The relatively short working distance of objective 1 precluded its use for some samples which were on thicker glass substrates. In those instances, objective 2 (NA = 0.7, 60X, Nikon) which had a larger working distance was used. L_D values as small as ∼200 nm could be determined with the convolution procedure from the images collected with objective 2.

The effect of depth-of-field on the fluorescence images was analyzed in detail. The near-field excitation creates a cone of PPEI singlet excitons which falls off exponentially with depth of penetration along the excitation axis and perpendicular to the focal plane of the objective. Linfoot and Wolf[30] have modeled the intensity distribution of a diffraction-limited image as a function of position along the axis perpendicular to the focus plane. Qualitatively, the diffraction image broadens with distance from the focal plane. In other words, a diffraction-limited image is broadened if the objective is defocused and, indeed, broadening of the spatial images reported herein was observed when the objective was defocused. To ensure focusing of the objective on the plane containing the most excitons, the objective was iteratively focused until the narrowest image was acquired. The image at the CCD is an integration of the images from all planes containing excitons. A numerical integration of

10140 *J. Phys. Chem. A, Vol. 103, No. 49, 1999*

Adams et al.
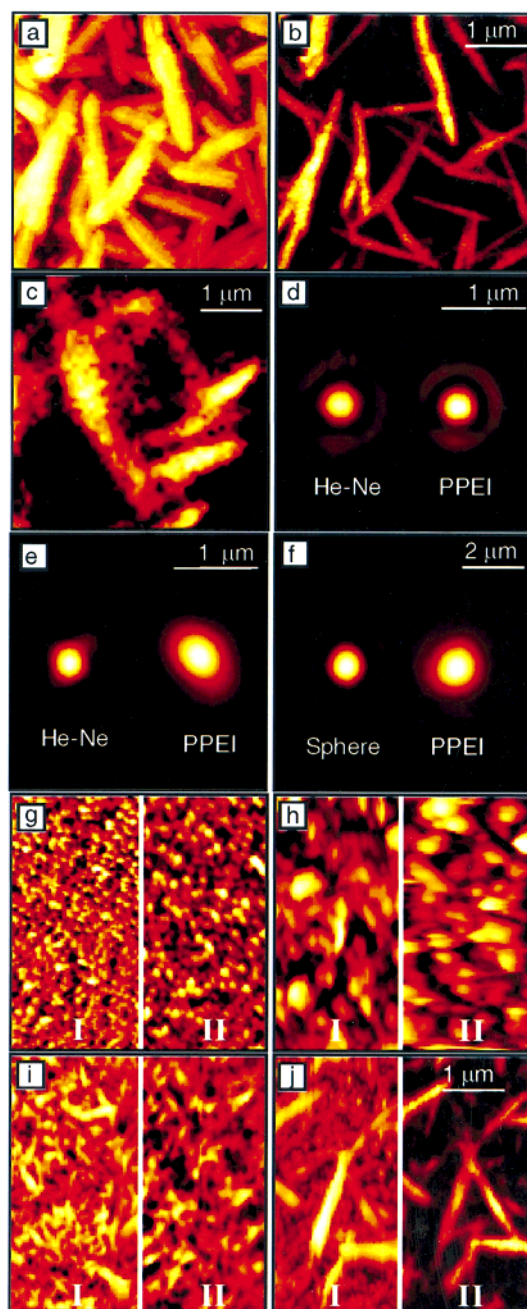
Figure 3. (a) Topography and (b) the simultaneously recorded near-field fluorescence image of PPEI microcrystals. (c) Far-field fluorescence imaging of PPEI microcrystals. Sample in (a–c) was solvent annealed extensively. (d) Spatial images of 633 nm HeNe laser from near field optical probe (left spot) and 680 nm emission (right spot) from a single PPEI microcrystal. (e) Spatial images of 633 nm HeNe laser (left spot) and 680 nm emission from a 150 nm thick PPEI film. (f) Spatial images of 680 nm emission from a 200 nm diameter fluorescent latex sphere (left spot) and a 50 nm thick PPEI film. (g) Topography of bare ITO and a PMT-coated ITO (I and II, respectively). (h) Topography of a 670 nm thick PPEI film on ITO and a 670 nm thick PPEI film on PMT-coated ITO (I and II, respectively). The samples were on the same underlying glass substrate and annealed under identical conditions. (i) Topography and fluorescence NSOM of a 24 nm thick PPEI film on bare ITO (I and II, respectively). (j) Topography and fluorescence NSOM of a 24 nm thick PPEI film on PMT-coated ITO (I and II, respectively). The samples in (i,j) were on the same underlying glass substrate and annealed under identical conditions. The scale is the same in (g–j). Images (a–d) were obtained with objective 1 and images (e–j) with objective 2.
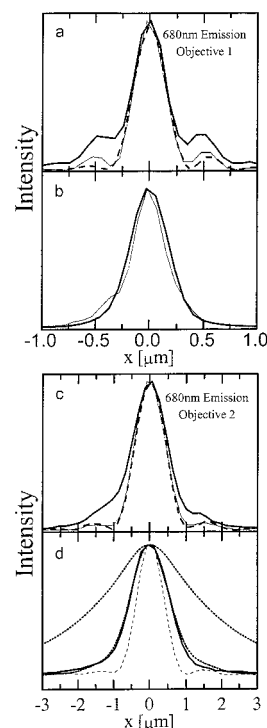
Figure 4. Linescans of spatial images of (a) 633 nm HeNe laser from a near-field probe (dashed line), 680 nm emission from a single 50 nm tall PPEI microcrystal (thin line), and 680 nm emission from a 50 nm thick PPEI film (thick line). (b) 680 nm emission from a 50 nm thick PPEI film (thin line) and a 150 nm thick PPEI film (thick line). (c) 680 nm emission from a 200 nm diameter fluorescent latex sphere (dashed line), 300 nm thick PPEI film (thin line), and 2400 nm thick PPEI film (thick line). (d) 633 nm HeNe laser from a near-field probe (dashed line), 600 nm thick PPEI film (thick line), and predicted linescans (see text) from PPEI films with exciton diffusion lengths of $L_D = 0.5$ μm and $L_D = 2.5$ μm (inner and outer dotted lines respectively). The line scans indicate intensity varitions along a horizontal axis through the maximal intensity of the spatial images, such as those in Figures 3d–f.

the Linfoot and Wolf intensity distribution, assuming a uniform distribution of PPEI excitons in a cone 600 nm high, showed that the broadening of the spatial image due to collection of all fluorescence in the cone is negligible.

Results and Discussion

Vapor deposited PPEI films of varying thickness in the range of 25–2400 nm were investigated. Films that were not subject to solvent annealing conditions were smooth (root-mean square = 3 nm by shear-force topography) and exhibited NSOM fluorescence images that were structureless and uniform. As described in detail in previous publications, annealing of PPEI samples under a vapor of methylene chloride produces a highly structured crystalline film. Simultaneous topographic and fluorescence NSOM images of an extensively annealed vapor deposited film are portrayed in Figures 3a and b. (The film thickness was ~30 nm prior to annealing.) The individual PPEI crystals are several microns long but only 10–100 nm wide and high. Under these annealing conditions, the topographic image reveals considerably wider crystals than the corresponding NSOM fluorescence image due to artifact in the topographic image resulting from the spatial convolution of a relatively flat NSOM tip with a sharp PPEI microcrystal.

It is interesting to compare the fluorescence NSOM image of this sample (Figure 3b) with a conventional far-field fluorescence image recorded with the CCD camera (Figure 3c)

Perylene Bis(phenethylimide) Thin Films

J. Phys. Chem. A, Vol. 103, No. 49, 1999 **10141**

and wide field epi-excitation (not shown in Figure 2). The individual PPEI crystals appear much sharper in the NSOM image due to the subdiffraction resolution of the NSOM technique.

We have taken advantage of the ability of NSOM to excite a small spatial region to measure L_D for a single microcrystal in the sample studied by Figures 3a-3c. The results are shown in Figure 3d. The spot on the right side of the Figure 3d is a fluorescence image of a single PPEI microcrystal ($\lambda_{ex} = 488$ nm; emission collected through 680 nm band-pass filter). For comparison the left spot in Figure 3d is the image of 633 nm light emitted from the same NSOM probe in feedback over the same PPEI sample without a band-pass filter in the collection optics. The 633 nm light is not absorbed by the PPEI crystal and the image is simply included as a reference to establish the spatial resolution of the instrument. (633 nm was chosen because the difference of its diffraction limited spot size with that of 680 nm is less than the resolution of the apparatus. The fluorescence maximum in the PPEI fluorescence spectrum is near 680 nm.)

A more quantitative analysis of the spatial profile of the fluorescence intensity has been obtained by recording line scans of the fluorescence intensity as a function of sample displacement, $I_{fl}(x)$, in various directions in the image plane. Line scans of the 633 nm HeNe laser spot (dashed line) and the 680 nm fluorescence from a PPEI microcrystal (thin line), Figure 4a, are indistinguishable within experimental error indicating that L_D for this PPEI microcrystal is unresolvably small (≤ 50 nm). The circular symmetry of the spot in Figure 3d is further indication of the absence of energy migration within experimental resolution, since spatially resolved energy diffusion would produce an asymmetric spot for a needle shaped microcrystal. Identical results were observed for all of the microcrystals that were investigated, indicating that $L_D \leq 50$ nm for this sample.

Figures 3d−f and 4a−d exhibit CCD fluorescence images and linescans of NSOM excited PPEI samples of various thickness, degrees of solvent annealing, on either glass or glass/ITO underlayers. Topographic and fluorescence NSOM images of these samples (e.g., Figures 3h−j) indicate that they are microstructured to varying degrees, even those exposed to short annealing periods, but in all cases are considerably more uniform than the exhaustively annealed sample described above.

As a second standard for the expected spatial profile of the fluorescence images of unresolvably small energy diffusion lengths, the spatial profile of a 200 nm diameter fluorescent latex sphere on a glass substrate was recorded (left spot in Figure 3f). The linescan of the fluorescence from a 300 nm thick PPEI film (thin line, Figure 4c) is indistinguishable, within experimental error, from the linescan of the fluorescence image of the sphere (dashed line, Figure 4c). However, several of the samples do exhibit fluorescence spots which differ significantly from the image of the HeNe light (633 nm) for the NSOM probe or the fluorescence of the latex sphere. For many of the PPEI samples the fluorescence spatial profiles are significantly broader than that for the HeNe, especially at the edges of the profile (for example, the PPEI images in Figure 3e−f). Similarly, the line scans of the fluorescent images of many films exhibit broadening relative to the linescans of the HeNe spot and small diameter latex sphere. Examples are shown in Figure 4a−d.

To quantitatively analyze the $I_{fl}(x)$ curves, we considered a simple one-dimensional steady-state diffusion model[19] that includes the combined effects of optical excitation, exciton diffusion, and singlet exciton decay, as follows.

$$\frac{\partial n(x,t)}{\partial t} = -\frac{n(x,t)}{\tau_s} + D\frac{\partial^2 n(x,t)}{\partial x^2} + pI_{ex}(x) \qquad (2)$$

Here x is displacement along the chosen direction of observation (in the sample x,y plane), $n(x,t)$ is the exciton density profile, p is the probability of absorption, and $I_{ex}(x)$ is the NSOM excitation light intensity profile.

We are interested in the steady-state solution of eq 2, which we denote by $n(x)$. Since exciton/exciton interactions can be ignored at the low excitation intensities of our experiments, $n(x)$ is given by eq 3, which is a convolution ($\otimes$) of $I_{ex}(x)$ with the solution, $n_\delta(x)$, to eq 2 for the case of excitation at a single point, i.e., a δ function.

$$n(x) = I_{ex}(x) \otimes n_\delta(x) \qquad (3)$$

Using standard methods[31] a numerical solution was obtained for $n_\delta(x)$.

Theoretical predictions for the observed fluorescence intensity profiles in Figure 4, i.e., $I_{fl}(x)$, can in principle be obtained by eq 4 as a convolution of $n(x)$ with the point-spread function $P(x)$ of the optical system (which due to diffraction is an Airy pattern).

$$I_{fl}(x) \propto n(x) \otimes P(x) \qquad (4)$$

However, a consideration of eqs 3 and 4, and the properties of the convolution operator, suggests an alternative approach which is used throughout this paper as outlined by eqs 5 and 6.

$$I_{fl}(x) \propto n_\delta(x) \otimes R(x) \qquad (5)$$

$$R(x) = I_{ex}(x) \otimes P(x) \qquad (6)$$

The advantage of this approach is that $R(x)$ can be estimated empirically by recording the intensity profile $I_{NSOM}(x)$ of the far-field image of the NSOM probe using a reference light source (e.g. the HeNe laser at 633 nm). Thus, $I_{NSOM}(x)$ reflects, for a particular sample/probe/optical system combination, the shape of the near field intensity profile, the effect of diffraction, and even the effects of certain optical artifacts and nonidealities.

For all of the samples investigated in this work the experimentally observed $I_{fl}(x)$ curves were considerably narrower than the theoretically predicted results for $L_D = 2.5$ μm. This is demonstrated in Figure 4d where the outermost dotted line represents the theoretical curve for $L_D = 2.5$ μm. Thus, this spatial imaging technique strongly suggests that singlet energy diffusion for PPEI does not occur on a 2.5 μm distance scale. The PPEI spatial images which exhibited the largest broadening were compared to simulated profiles. This comparison (Figure 4d) led to a value of ~500 nm for L_D. This value is only a factor of 2 greater than the reported $L_D = (225 \pm 15)$ nm for 3,4,9,10-perylenetetracarboxylic dianhydride (PTCDA)[22] which is structurally similar to PPEI. However, the energy diffusion constant D_s implied by $L_D = 500$ nm for PPEI is ~7 cm²/s which is ~100 times larger than the corresponding value for PTCDA. (The singlet lifetime of PPEI is 350 ps[8] while that of PTCDA is ~4 ns.[32] See eq 1.) The exciton diffusion length for PTCDA was obtained by a photoconduction method that measures the effect of exciton diffusion on the photocurrent of a prototypical solar cell device.

The microstructure of selected PPEI films are shown in Figures 3h−j. Samples exposed to even short periods of annealing exhibit a dense composite of microcrystals with typical dimensions: $l = 1000$ nm, $w = 100$ nm, $h = 50$ nm.

The observation that these samples exhibit $L_D \approx 500$ nm suggest that energy must migrate from microcrystal to microcrystal during the diffusion process, if L_D is indeed as long as 500 nm.

An experiment was conducted to elucidate the role of oxygen in exciton diffusion in PPEI. A CCD fluorescence image of NSOM excited PPEI was obtained under ambient conditions. The enclosed NSOM apparatus was then purged with nitrogen and CCD fluorescence images were recorded after 30 and 45 min of continuous purging. The images were virtually identical with the image taken in the presence of air indicating oxygen does not appreciably quench singlet excitons in PPEI.

It may be that the broadening in the fluorescence spatial profiles for PPEI is not actually due to energy migration but rather some unidentified optical artifact. For example, thin films can act as waveguides in propagating amplified spontaneous emission in the plane of the film.[33] The highly refractive and microstructured PPEI films may trap PPEI fluorescence light for hundreds of nanometers which is then scattered to the far field and detected. A potential complication with this method for L_D determination is that this optical artifact observed for structured samples can distort and broaden the fluorescence image "spot" and thus lead to an overestimation of L_D. Thus, the L_D values may be an overestimate of the migration lengths since the most obvious potential sources of error would lead to an overestimate of the energy migration length.

Another potential complicating factor in the use of NSOM to measure exciton diffusion lengths is perturbation of the exciton lifetime by the metal coating of the NSOM probe. For example, aluminum-coated NSOM probes have been shown to perturb fluorescence lifetimes of single molecules by both radiative and nonradiative mechanisms.[34] However, our previous report that the fluorescence lifetime of PPEI films are the same under far-field excitation and near-field, suggests that NSOM probe perturbations are not a significant factor for our PPEI samples.[8] As a further test of the effect of the NSOM probe on the PPEI emission, the fluorescence lifetime and the fluorescence images of a 300 nm thick PPEI film were recorded with the NSOM probe at two different distances above the sample surface, i.e., ~ 7 nm and 50−60 nm. (The 50−60 nm results were recorded during slow retraction of the probe and were not in shear force feedback.) The fluorescence lifetimes (~ 350 ps) and spatial image of the exciton emission (far field) were indistinguishable for the two distances. These results suggest probe perturbation of the PPEI exciton lifetime and diffusion is negligible.

The spatial imaging method used in this paper involved much greater excitation intensities than the fluorescence quenching method.[6] High excitation intensities may photogenerate trapped charges which can act as exciton quenchers. This would lead to an underestimation of L_D. To address this possibility, spatial images were obtained by varying the excitation intensity by a factor of 100. The resulting images and corresponding linescans were identical, within experimental error, suggesting trapped charges are not significant quenchers. However, it should be noted that the weakest excitation energy employed in these experiments was still greater than that employed with the fluorescence quenching technique. We cannot unequivocally rule out that even the "weak" excitation used in these experiments leads to a saturated trapped charge concentration.

The discrepancy between the previous report of $L_D = (2.5 \pm 0.5)$ μm for solvent-annealed PPEI and the results reported herein may be due to the tremendous inhomogeneity and restructuring of PPEI that results from solvent annealing. In the previous results the degree of fluorescence quenching in a

multilayer structure was determined by measuring the ratio of the fluorescence intensity of annealed PPEI on a PMT/ITO/glass multilayer to a "reference" of annealed PPEI on ITO/glass. The PMT acts as a exciton quencher at the PPEI/PMT interface.[35] However, a comparison of topographic and NSOM images of PPEI films annealed under identical conditions (Figures 3i,j) reveals that the underlying layers can actually influence the microstructure of the PPEI overlayer. The PPEI on PMT/ITO/glass (Figure 3j) consists of longer, needle-shaped microstructures than the PPEI on ITO/glass (Figure 3i). In addition, the PPEI surface coverage is considerably less on the PMT/ITO/glass. Thus, the PPEI/ITO/glass region of the sample may not be an ideal "reference" for the fluorescence intensity.

Figure 3g shows the topography of an ITO/glass substrate as well as the topography of PMT coated (~100 nm) onto the same ITO/glass substrate. The PMT coating exhibits a similar morphology to the underlying ITO layer. The topography of a 670 nm thick PPEI film on ITO/glass and on PMT/ITO/glass is shown in Figure 3h. The films were annealed under identical conditions. Unlike the thin 24 nm PPEI film (Figure 3i-j), the underlying PMT layer has only a modest effect on the topography of the relatively thick PPEI layer.

Conclusions and Summary

The distance over which singlet energy is transferred in polycrystalline films of perylene bis(phenethylimide) (PPEI) was measured by an imaging technique with a resolution of ≥ 50 nm. The excitation source was a near-field Al coated optical fiber probe with an optical field diameter of ~50 nm. The steady-state PPEI emission was imaged in the far field with the CCD camera while the tip position of the sample was held at a fixed position on the sample. Energy migration lengths were observed to vary in the range of ≤ 50 to 500 nm depending on film morphology and thickness. The film morphologies were characterized by fluorescence NSOM and scanning force microscopy. The singlet energy migration lengths reported herein are considerably smaller that the 2.5 μm value recently reported.

References and Notes

(1) Shen, Z. L.; Burrows, P. E.; Bulovic, V.; Forrest, S. R.; Thompson, M. E. *Science* **1997**, *276*, 2009−2011.

(2) Simon, J.; Andre, J.-J. *Molecular Semiconductors*; Springer-Verlag: Berlin, 1985.

(3) Aziz, H.; Popovic, Z. D.; Hu, N.-X.; Hor, A.-M.; Xu, G. *Science* **1999**, *283*, 1900−1902.

(4) Law, K.-Y. *Chem. Rev.* **1993**, *93*, 449−486.

(5) Gregg, B. A. *J. Phys. Chem.* **1996**, *100*, 852−859.

(6) Gregg, B. A.; Sprague, J.; Peterson, M. W. *J. Phys. Chem. B* **1997**, *101*, 5362−5369.

(7) Adams, D. M.; Kerimo, J.; Olson, E. J. C.; Zaban, A.; Gregg, B. A.; Barbara, P. F. *J. Am. Chem. Soc.* **1997**, *119*, 10608.

(8) Conboy, J. C.; Olson, E. J. C.; Adams, D. M.; Kerimo, J.; Zaban, A.; Gregg, B. A.; Barbara, P. F. *J. Phys. Chem. B* **1998**, *102*, 4516.

(9) Cormier, R. A.; Gregg, B. A. *J. Phys. Chem. B* **1997**, *101*, 11004−11006.

(10) Cormier, R. A.; Gregg, B. A. *Chem. Mater.* **1998**, *10*, 1309−1319.

(11) Chandrasekhar, S. *Rev. Mod. Phys.* **1943**, *15*, 1−89.

(12) Kirkaldy, J. S.; Young, D. J. *Diffusion in the Condensed State*; Institute of Metals: London, 1987.

(13) Kenkre, V. M.; Parris, P. E.; Schmid, D. *Phys. Rev. B* **1985**, *32*, 4946−4955.

Perylene Bis(phenethylimide) Thin Films

J. Phys. Chem. A, Vol. 103, No. 49, 1999 **10143**

(14) Swenberg, C. E.; Geacintov, N. E. Exciton interactions in organic solids. In *Organic Molecular Photophysics*; Birks, J. B., Ed.; Wiley: London, 1973; Vol. 1, pp 489−564.

(15) Borsenberger, P. M.; Weiss, D. S. *Organic Photoreceptors for Imaging Systems*; Marcel Dekker: New York, 1993.

(16) Ghosez, P.; Cote, R.; Gastonguay, L.; Veilleux, G.; Denes, G.; Dodelet, J. P. *Chem. Mater.* **1993**, *5*, 1581−1590.

(17) Sims, T. D.; Pemberton, J. E.; Lee, P.; Armstrong, R. *Chem. Mater.* **1989**, *1*, 26−34.

(18) Klofta, T. J.; Danziger, J.; Lee, P.; Pankow, J.; Nebesny, K. W.; Armstrong, N. R. *J. Phys. Chem.* **1987**, *91*, 5646−5651.

(19) Kenkre, V. M.; Wong, Y. M. *Phys. Rev. B* **1980**, *22*, 5716−5722.

(20) Birks, J. B. *Photophysics of Aromatic Molecules*; Wiley-Interscience: New York, 1970.

(21) Popovic, Z. D.; Hor, A.-M.; Loutfy, R. O. *Chem. Phys.* **1988**, *127*, 451−457.

(22) Bulovic, V.; Forrest, S. R. *Chem. Phys.* **1996**, *210*, 13−25.

(23) Simpson, O. *Proc. R. Soc. London* **1957**, *A238*, 402−411.

(24) Takahashi, Y.; Tomura, M. *J. Phys. Soc. Jpn.* **1971**, *31*, 1100−1108.

(25) Powell, R. C. *Phys. Rev. B* **1970**, *2*, 2090−2097.

(26) Heller, W.; Filoramo, A.; Roussignol, P.; Bockelmann, U. *Solid-State Electron.* **1996**, *40*, 725−728.

(27) Vanden Bout, D. A.; Kerimo, J.; Higgins, D. A.; Barbara, P. F. *J. Phys. Chem.* **1996**, *100*, 11843−11849.

(28) Reid, P. J.; Higgins, D. A.; Barbara, P. F. *J. Phys. Chem.* **1996**, *100*, 0, 3892−3899.

(29) Higgins, D. A.; Barbara, P. F. *J. Phys. Chem.* **1995**, *99*, 3−7.

(30) Linfoot, E. H.; Wolf, E. *Proc. Phys. Soc.* **1956**, *69*, 823−832.

(31) Crank, J. *The Mathematics of Diffusion*, 2nd ed.; Clarendon: Oxford, 1975.

(32) Gomez, U.; Leonhardt, M.; Port, H.; Wolf, H. C. *Chem. Phys. Lett.* **1997**, *268*, 1−6.

(33) Denton, G. J.; Tessler, N.; Stevens, M. A.; Friend, R. H. *Adv. Mater.* **1997**, *9*, 547−551.

(34) Bian, R. X.; Dunn, R. C.; Xie, X. S. *Phys. Rev. Lett.* **1995**, *75*, 4772−4775.

(35) Noma, N.; Tsuzuki, T.; Shirota, Y. *Adv. Mater.* **1995**, *7*, 647−648.